The nonlinear optical, magnetic, and Mössbauer spectral properties of some iron(III) doped silica xerogels

L. REBBOUH, V. ROSSO, Y. RENOTTE, Y. LION, F. GRANDJEAN*
Department of Physics, B5, University of Liège, B-4000, Sart-Tilman, Belgium
E-mail: fgrandjean@ulg.ac.be

B. HEINRICHS, J.- P. PIRARD
Laboratoire de Génie Chimique, Department of Applied Chemistry, B6a, University of Liège, B-4000, Sart-Tilman, Belgium

J. DELWICHE, M.-J. -HUBIN-FRANSKIN
Department of Chemistry, B6c, University of Liège, B-4000, Sart-Tilman, Belgium

GARY J. LONG
Department of Chemistry, University of Missouri-Rolla, Rolla, Missouri 65409-0010, USA

Published online: 21 April 2006

Iron(III) species dispersed in silica have been synthesized with a sol-gel process. The iron(III) was introduced as the acetylacetonate complex into a solution of tetraethoxysilane to yield, after evaporative drying, pellets or monoliths. Two gels were dried very slowly over a period of five months in order to prepare a defect free monolith useful for nonlinear optical studies. *Z*-scan experimental studies on the resulting, transparent, monolithic, doped solid revealed an optical Kerr effect, a third order nonlinear optical phenomenon showing a linear dependence of the refractive index on the irradiance with a nonlinear refractive index, n_2, of -1.95×10^{-11} cm^2/W. Magnetic susceptibility studies between 4.2 and 295 K revealed paramagnetic behavior with a Curie constant of 4.433 (emu/mol)K and a Weiss temperature of -7.1 K. Magnetization studies at 5 K and at applied fields of up to 4 T and Mössbauer spectral studies between 4.2 and 295 K revealed a 50:50 mixture of paramagnetic species and nanoparticles with an average particle radius of 1.3 ± 0.2 nm. A blocking temperature of 70 K and a magnetic anisotropy energy of 2.4×10^5 J/m^3 are derived from the Mössbauer spectra.
© *2006 Springer Science + Business Media, Inc.*

1. Introduction

Nanocomposite materials containing iron nanoparticles are of interest both because of their promising electrical, magnetic, and optical properties and because of their potential specific applications in photonics [1–3], catalysis [4–7], magnetic recording [8], and biological sensors. Tailoring the size distribution of the nanoparticles is a difficult problem, a problem that may be solved by dispersing the nanoparticles into an inorganic matrix. Silica aerogels and xerogels are good potential inorganic host materials because of their excellent efficiency as thermal, electrical, and acoustic insulators.

The sol-gel process is generally viewed as a chemical process involving first the formation of a sol followed by a gel, which is a biphasic material with a solid encapsulating a solvent [4]. If the encapsulated liquid is removed from the gel by evaporative drying, the resulting solid is known as a xerogel. The sol-gel method is a particularly efficient technique for dispersing metal salts or metal complexes at the molecular or cluster level into an organic or inorganic matrix. Indeed, one needs "only" to introduce the desired species into the precursory solution of the final gel.

*Author to whom all correspondence should be addressed.
0022-2461 © *2006 Springer Science + Business Media, Inc.*
DOI: 10.1007/s10853-006-6336-3

Dissolved in the initial solution, the species will finally be homogeneously distributed into the resulting gel.

In this study the nonlinear optical properties of an iron(III) doped silica xerogel are determined by the *Z*-scan method. The magnetic properties have been determined both by SQUID and vibrating sample magnetometry, and the iron-57 Mössbauer spectral properties have been measured between 4 and 295 K.

2. Experimental

2.1. Precursor solution

A 250 ml sample of the wet gel has been synthesized by the following procedure. A 2.18 g sample of iron(III) acetylacetonate powder, $Fe(acac)_3$ or $Fe[CH_3COCH{=}C(O\text{-})CH_3]_3$, obtained from Aldrich with 97% purity, is placed in 81 ml of ethanol, obtained from Merck with 99.8% purity. The resulting slurry is stirred at room temperature until a clear red solution is obtained after about 4 h. Then 62 ml of tetraethoxysilane $Si(OC_2H_5)_4$, TEOS, obtained from Merck with 98% purity, is added. Finally, a solution containing 25 ml of aqueous 0.2 N NH_3 dissolved in 81 ml of ethanol is slowly added with vigorous stirring. The values of the hydrolysis ratio, i.e., the molar ratio $H = [H_2O]/[TEOS]$, and of the dilution ratio, i.e., the molar ratio $R = [C_2H_5OH]/[TEOS]$, are 5 and 10, respectively.

The amount of tetraethoxysilane and $Fe(acac)_3$ have been chosen in order to yield to 2 weight percent of iron(III) in the final dried and calcined Fe_2O_3/SiO_2 xerogel. Hence in all the uncalcined samples studied herein, the iron(III) content is expected to be less than 2 weight percent.

2.2. Gelation

Three different samples were prepared by different drying methods; the three samples are designated as Fe-1, Fe-2, and Fe-3 herein. For Fe-1, part of the precursor solution, prepared as described above, is transferred into a glass flask which is then tightly sealed and heated to 70°C for 3 days for gelation and aging [9]. A gel time of ca. 4 h is observed for the sample, where the gel time is the elapsed time between the introduction of the last reactive component to the solution and gelation, which corresponds to the time at which the liquid no longer flows when the flask is tilted. For Fe-2 and Fe-3, part of the precursor solution was transferred into two 10 mm pathlength Camlab KL/1938 visible range polystyrene spectrophotometer cuvettes of $30 \times 10 \times 5$ mm^3 volume and then covered with parafilm. Gelation and aging were then carried out at 293 K, a temperature at which ca. 8 days are required for gelation.

2.3. Drying

For Fe-1, the above prepared gelation product was dried by placing the open reaction flask in a vacuum drying oven at one atmosphere and 353 K. Next, in order to prevent gel bursting, the pressure was slowly reduced over a period of 90 h to 1200 Pa. The sample was then heated to and maintained at 423 K for 72 h. The resulting rapid drying produces cracks in the gel and leads to a xerogel in the form of transparent red pellets of irregular thickness, a form that makes Fe-1 suitable for the Mössbauer spectral studies reported herein, but unsuitable for the nonlinear optical studies.

For the nonlinear optical studies a thin monolith with no cracks and with a constant thickness is required. Therefore, in order to avoid the appearance of cracks in the resulting gels, Fe-2 and Fe-3, were dried very slowly and differently in the two separate cuvettes, described above. The first cuvette was maintained at 293 K for five months with parafilm covering the top, after five months the parafilm was removed and the cell was placed in a drying oven at 343 K and atmospheric pressure for 24 h. This procedure yielded a xerogel, Fe-2, that is a perfect, transparent, red, monolith with no cracks and with a thickness of 2.14 mm, a form which made it usable for the nonlinear optical measurements reported herein. A portion of this sample was crushed and used for the SQUID magnetometry studies reported herein. The second cuvette was also maintained at 293 K for five months but with a small hole in its parafilm covering. In contrast to the first cuvette, this procedure yielded a xerogel, Fe-3, that was cracked but acceptable for the magnetization studies reported herein.

The properties of the iron(III) doped xerogels studied herein will be compared with previously studied iron(III) doped xerogels and aerogels. In the earliest studies [10, 11], the source for iron(III) was iron nitrate and a high iron(III) content of 25 weight percent was achieved in the doped xerogels and aerogels. More recently, $Fe(acac)_3$ has been used as a source for iron(III) and doping levels of 3 [12] and 20 [7] weight percent have been obtained.

2.4. Z-scan nonlinear optical studies

The third-order nonlinear optical properties of the transparent monolithic iron(III) doped xerogel, Fe-2, were measured by the *Z*-scan technique [1, 13], see Fig. 1a. The studies used a 1550 nm 100 femtosecond mode locked fiber laser with a 20 MHz repetition rate and a mean power of 15 mW incident upon the sample. The Gaussian laser beam parameters of 60 μm for the beam cross-sectional waist, W_0, and 9.9 mm for the Rayleigh length, Z_0, were determined with a Beamscan 1180 beam analyzer obtained from Photon Inc.

2.5. Magnetic studies

The mass magnetization of the iron(III) doped xerogel powder, Fe-3, was measured at 295 and 5 K in fields of up to 4 T with an Oxford Instruments Maglab VT9 vibrating sample magnetometer. The zero field cooled magnetic susceptibility of crushed Fe-2 was measured between 4

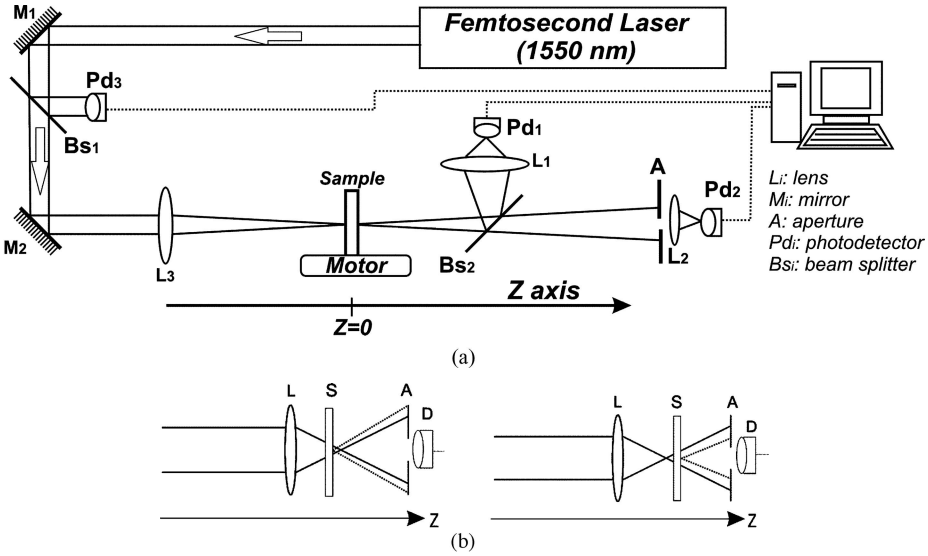

Figure 1 (a) A schematic diagram of the *Z*-scan experimental technique used to determine the nonlinear optical properties of the iron(III) doped silica xerogel. (b) A nonlinear optical sample, *S*, placed before, left, and after, right, the focus of a convergent lens, *L*, where *A* is the aperture, and *D* is the PD_2 detector.

and 300 K in an applied field of 0.002 T with a Quantum Design MPMS XL7 SQUID magnetometer.

2.6. Density determination

The bulk density, ρ, of the iron(III) doped xerogel was measured by mercury pycnometry and found to be 1009 ± 50 kg/m^3.

2.7. Mössbauer spectroscopy

The iron-57 Mössbauer spectra of the Fe-1 iron(III) doped xerogel have been measured between 4.2 and 295 K on a constant acceleration spectrometer which utilized a rhodium matrix cobalt-57 source and was calibrated at 295 K with α-iron foil. The isomer shifts are reported relative to α-iron at 295 K. The absorber thickness was 350 mg/cm^2 of sample or 3.5 mg/cm^2 of natural abundance iron. The hyperfine fields, isomer shifts, paramagnetic quadrupole splittings, line widths, and relative areas have relative errors of 0.3 T, 0.005, 0.01, and 0.01 mm/s, and 1 percent; the absolute errors are approximately twice these values.

3. Results and discussion

3.1. Nonlinear optical studies

The third-order nonlinear optical phenomenon, also known [1–3] as the optical Kerr effect, results from the linear dependence, $n = n_0 + n_2 I$, of the refractive index, n, of a material on the irradiance, I, in W/cm^2, where n_0 is the linear refractive index and n_2 is the nonlinear refractive index in cm^2/W. The Z-scan method [1, 13], a method which determines both the nonlinear absorption and the nonlinear refraction [13], has been used to determine the nonlinear refractive index of the Fe-2 transparent monolithic iron(III) doped xerogel. This technique is based on the variation of the refractive index that arises when a nonlinear optical material is irradiated by a strong Gaussian laser beam in the TEM_{00} mode [2]. Many different mechanisms [1–3], such as resonance, molecular orientation, saturated or saturable absorption, reverse saturable absorption, and multi-photon absorption, may account for the variation in the refractive index and complementary experimental techniques are often required to unambiguously determine the actual mechanism appropriate for a given material.

When a strong electric field is applied to a material, the macroscopic polarization, P, of the material may be expressed [1, 2] in powers of E, the applied electric field as

$$P = \varepsilon_0 \chi^{(1)} : E + \varepsilon_0 \chi^{(2)} : E^2 + \varepsilon_0 \chi^{(3)} : E^3 + \cdots, \qquad (1)$$

where $\chi^{(n)}$ is the n-th order susceptibility, a tensor of order $n + 1$, the colons indicate a tensorial product with the electric field, the first term represents the linear polarization, and the subsequent terms represent higher order contributions to the polarization.

If a centrosymmetric material is irradiated with a Gaussian laser beam and exhibits an optical Kerr effect, its refractive index, n, obeys the expression,

$$n = n_0 + n_2 I, \qquad (2)$$

where I is the irradiance and n_0 and n_2 are, respectively, the linear and nonlinear portions of the refractive index; the material is then referred to as a Kerr optical material.

Imagine that a Kerr optical material is situated at the *Z*-point of an optical axis, see Fig. 1a. When a laser beam passes through the sample, the refractive index of the material located in the center of the laser beam will vary

from that located at the edge of the laser beam because of the Gaussian radial distribution of the irradiance of the laser beam. The material then has a radial gradient in its refractive index, a gradient that produces a non-uniform phase shift in the laser electromagnetic wave. As a consequence, the material behaves either as a convergent lens, for $n_2 > 0$, or a divergent lens, for $n_2 < 0$.

The *Z*-scan technique, see Fig. 1a, consists of moving the sample, *S*, to both sides, $\pm$ *Z*, of the focal point at $Z = 0$ of the convergent lens, L_3, along the *Z*-propagation axis. The emergent laser beam passes through a circular aperture, *A*, far from the focus, and a detector, PD_2, measures the transmitted irradiance. For each $\pm$ *Z*-position of the sample near the focal point, the lensing induced inside the material has a specific focal length that depends upon the Gaussian radial profile of the irradiance of the incident laser beam, see Fig. 1b.

For a positive n_2 and a negative sample position, –*Z*, the transmitted beam at the aperture is radially broader than the beam in the absence of a sample and the irradiance transmitted through the aperture is reduced, see the left side of Fig. 1b. In contrast, for a positive n_2 convergent lens and a positive sample position, $+Z$, the transmitted beam at the aperture is radially narrower than the beam in the absence of a sample and the irradiance transmitted through the aperture is increased, see the right side of Fig. 1b. A similar reasoning applied to a divergent photoinduced lens leads to the reverse change in the irradiance.

The irradiance transmitted through the aperture, normalized to the transmitted irradiance of the sample placed far from the focus at a large $\pm$Z, at which point the nonlinear n_2 term becomes negligible, is recorded as a function of *Z* normalized by Z_0, i.e., Z/Z_0, where Z_0 is the Rayleigh length of the laser beam. The sign of the nonlinearity is determined by the relative position of the maximum and the minimum in the *Z*-scan curve. If a minimum in the normalized transmittance is followed by a maximum then $n_2 > 0$, whereas if a maximum is followed by a minimum then $n_2 < 0$. If the curve obtained by *Z*-scan method contains only nonlinear refraction, we can use the method developed by Van Stryland and Sheik-Bahae [13] to determine the nonlinear refractive index, n_2, by measuring the difference of the normalized transmittance between the maximum and the minimum. The method used to calculate n_2 for samples studied on the experimental facilities used herein is discussed in detail elsewhere [14]. The n_2 value can also be determined in the presence of nonlinear absorption if the nonlinear absorption can be measured separately in an "open aperture" Z-scan experiment [13, 14] by the photodetector PD_1, see Fig. 1a, and the ratio of the normalized "closed aperture" transmittance, measured by the photodetector PD_2, to the "open aperture" *Z*-scan transmittance will reflect only the nonlinear refraction process.

The *Z*-scan normalized transmittance, obtained for the Fe-2 transparent monolithic iron(III) doped xerogel, is shown in Fig. 2. In this figure the large points represent the experimental transmittance through aperture *A* as detected by the PD_2 photodetector, a "closed aperture *Z*-scan," and is the product of the nonlinear refraction and the nonlinear absorption. The solid curve corresponds to a fit of the experimental transmittance with the model [13] of Van Stryland and Sheik-Bahae. The small dotted curve in Fig. 2 represents the nonlinear absorption as measured by detector PD_1, an "open aperture *Z*-scan." The dashed curve in Fig. 2 is the ratio of the solid curve transmittance to the small dotted curve transmittance and corresponds to the contribution of nonlinear refraction. In this dashed curve, the maximum followed by the minimum in the normalized transmittance corresponds to a photoinduced defocusing lens, i.e., $n_2 < 0$, for the transparent monolithic iron(III) doped xerogel. From the difference in transmittance between the maximum and the minimum, a value of -1.95×10^{-11} cm^2/W is obtained for the nonlinear refractive index, n_2, of the Fe-2 iron(III) doped xerogel. This value is rather large for metallic ions encapsulated in a substrate such as a xerogel.

It is apparent from the small dotted curve in Fig. 2 that a nonlinear absorption is also present in the doped xerogel, a nonlinear absorption that also gives rise to some nonlinear refraction. A linear absorption spectrum of the sample, not shown, exhibits a maximum in the absorbance at ca. 500 nm. Consequently, the nonlinear absorption occurs because the wavelength of the 1550 nm laser beam produces a multi-photon transition in the sample, specifically, a three-photon absorption transition. However, a difference of approximately an order of magnitude is observed between the nonlinear absorption curve and the nonlinear refraction curve, see Fig. 2. The large nonlinear refraction effect compared with the small nonlinear absorption indicates that a mechanism other than nonlinear absorption gives rise to the observed nonlinear refraction. The possibility of thermal lensing [15] can be eliminated because of the short, 100 femtosecond, duration of the pulse.

Based on the sample synthesis starting with the iron(III) acetylacetonate complex, $Fe(acac)_3$, and the low drying temperatures used herein for Fe-2, we can assume that at least some of the iron(III) ions are still associated with the acetylacetonate ligands, ligands which contain partially delocalized electrons. Thus the large observed nonlinear refraction may arise, at least in part, from a change in the molecular dipole moment associated with the mobility of these electrons and their response to the large electric field of the laser radiation and, consequently, a change in the local refractive index occurs [1, 3]. Indeed, a reorganisation or movement of the electric charges associated with either the acetylacetonate ligands or the oxide dianions toward the iron(III) ion may occur in the presence of a strong polarizing electric field.

3.2. Magnetic studies

The magnetic susceptibility of the iron(III) doped silica xerogel has been measured from 4.2 to 300 K in an ap-

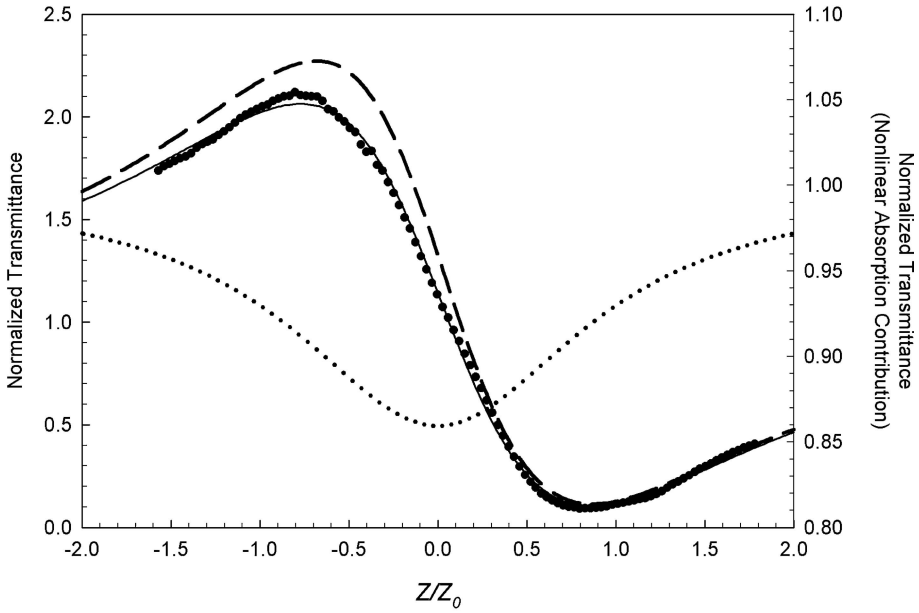

Figure 2 The *Z*-scan results obtained for the iron(III) doped silica xerogel, where the larger points correspond to the normalized transmittance measured by photodetector PD_2, left scale, the continuous curve corresponds to a fit with the model developed by Van Stryland and Sheik-Bahae, ref. 13, left scale, the small points correspond to the contribution of nonlinear absorption measured by photodetector PD_1, right scale, and the dashed curve corresponds to the contribution of the nonlinear refraction derived from the division of the solid curve transmittrance by the small dotted curve transmittance. The maximum followed by a minimum in the nonlinear refraction with increasing Z/Z_0 is the result of photoinduced divergent lensing. The order of magnitude difference in the left and right transmittance scales should be noted.

plied field of 10.002 T after cooling over a period of ca. one hour from room temperature to 4.2 K in a zero applied field. Subsequently, the magnetic susceptibility has been measured from 300 to 4.2 K in an applied field of 50.002 T. On warming and subsequent cooling the xerogel exhibits identical Curie law magnetic behavior with a Curie constant, C, of 4.433 (emu/mol Fe)K and a Weiss temperature, θ, of –7.1 K, and, as is shown in the inset to Fig. 3, a plot of the inverse molar magnetic susceptibility, $1/\chi_M$, is linear between 4 and 300 K. In obtaining the molar magnetic susceptibility the iron(III) content, which is expected to be less than 2 weight percent for the wet sample, has been reduced to 1.0 weight percent, a value that yields an effective magnetic moment of 5.95 μ_B. This moment is consistent with the expected paramagnetic spin-only iron(III) effective magnetic moment of 5.92 μ_B. As may be observed in Fig. 3, the effective moment remains essentially constant between 30 and 300 K, but increases somewhat below ca. 30 K to a maximum of 8.3 μ_B at 4 K. This increase results from short-range ferromagnetic exchange correlations, correlations that are also observed in the Mössbauer spectra to be discussed below.

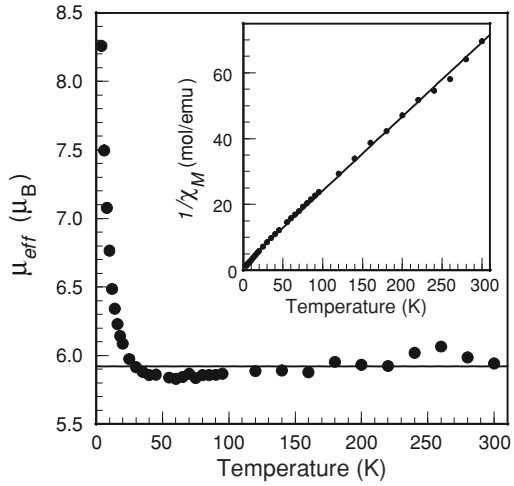

Figure 3 The temperature dependence of the effective magnetic moment of the iron(III) doped silica xerogel measured in an applied field of 0.002 T after slowly cooling from room temperature to 4 K in a zero applied field. Inset. The temperature dependence of $1/\chi_M$, fit with the Curie-Weiss law.

The identical field cooled and zero-field cooled temperature dependence of the magnetization obtained herein differs markedly from the temperature dependence reported [11, 12] for iron(III) oxide doped aerogels and xerogels. For γ-Fe_2O_3 doped xerogels with an average particle size of 5 nm, a maximum at ca. 70 K is observed [11] in the zero-field cooled measurements, whereas for a ferrihydrite doped aerogel with an average particle size of 5 nm, a maximum at ca. 45 K is observed [12] in the zero-field cooled measurements. In contrast, the temperature dependence of the inverse molar susceptibility shown in Fig. 3 is similar to that observed [8] for the 10 percent Fe_2O_3 doped aluminosilicate glass-ceramics. Hence, a wide variety of magnetic behavior has been observed in different iron(III) doped xerogels and aerogels, behavior that depends both on the material used as the iron source and on the preparation process used.

The mass magnetizations measured in applied fields of up to ±4 T between 100 and 295 K are linear and, as would be expected for a paramagnetic compound, exhibit no magnetic hysteresis. The mass magnetizations measured at 295 and 100 K, have been fit between ±4 T with a linear relationship, $M = \chi' H$, and the slopes, χ', of 0.03798(5) and 0.09651(4) (Am^2/kg)/T, respectively, correspond to the unitless magnetic susceptibilities, χ, of $48.16(6) \times 10^{-6}$ and $122.37(5) \times 10^{-6}$. The mass magnetizations measured at 5 K between ± 1 T are also linear and the resulting slope, χ', of 1.552(3) (Am^2/kg)/T corresponds to the unitless magnetic susceptibility, χ, of $1968(2) \times 10^{-6}$. The mass magnetizations obtained between 0 and 4 T are shown in Fig. 4.

The mass magnetization measured at 5 K between ±4 T indicates that the iron(III) doped silica xerogel exhibits short-range ferromagnetic exchange at this temperature, as is also observed by Mössbauer spectroscopy, see below. The mass magnetization is not saturated at 5 K in an applied field of ±4 T and indicates that the magnetic entities are either nanoparticles or molecular clusters, or a mixture of superparamagnetic particles and isolated paramagnetic iron(III) ions, as is indicated by the Mössbauer spectra, see below.

Different fits of the mass magnetization in Am^2/kg obtained at 5 K have been undertaken to identify the magnetic nature of the iron(III) doped xerogel and to obtain an estimate of the size of the nanoparticles. First, a fit was carried out with the Langevin function,

$$L(V\rho M_s H/kT) = M_s[\coth(V\rho M_s H/kT) - kT/V\rho M_s H], \quad (3)$$

where V is the average volume of the magnetic particles in m^3, ρ is 1009 kg/m^3, the density of the particles, M_s is the saturation magnetization in Am^2/kg, k is the Boltzmann constant in J/K, T is the temperature in K, and H is the applied field in T. This fit yields an M_s of 6.4 ± 0.1 Am^2/kg and a V of $(8.0 \pm 0.1) \times 10^{-27} m^3$ or 8 ± 1 nm^3 for the magnetic particles, a volume which corresponds to an average particle radius of 1.2 ± 0.1 nm if one assumes the presence of monodispersed spherical nanoparticles.

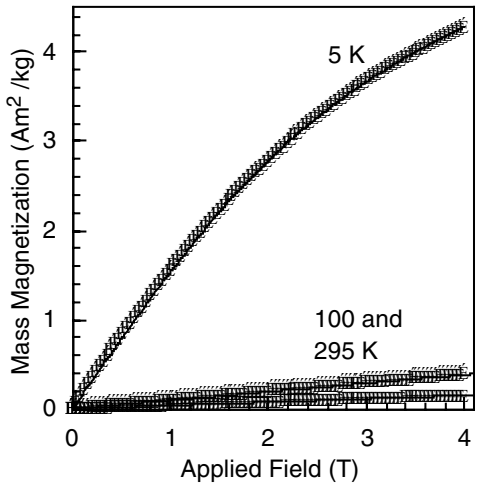

Figure 4 The temperature dependence of the mass magnetization of the iron(III) doped silica xerogel measured at 5, 100, and 295 K. A fit with a Langevin function is shown as the solid line through the 5 K data.

Second, a fit was attempted with the Brillouin function,

$$M = N_g J \mu_B \quad B_J(gJ\mu_B H/kT), \quad (4)$$

where $B_J(x)$ is given by

$$B_J(gJ\mu_B H/kT) = \frac{2J+1}{2J}\coth\left(\frac{(2J+1)gJ\mu_B H}{2JkT}\right) - \frac{1}{2J}\coth\left(\frac{gJ\mu_B H}{2JkT}\right),$$

and N is the number of magnetic atoms or ions per kg, g is the Landé factor, J is 5/2 for iron(III) ions, and μ_B is the Bohr magneton in Am^2. The resulting fit was much poorer than the Langevin fit. This poor fit indicates that the iron(III) doped xerogel is not a simple paramagnetic substance.

Third, by assuming that the sample is a mixture of superparamagnetic particles and isolated paramagnetic iron(III) ions, a fit with a linear combination of the Langevin and the Brillouin functions, i.e., a fit with the expression

$$M(H) = (1-c)L(H/kT) + cB(H/kT) \quad (5)$$

was attempted. The fitting procedure did not converge if the coefficient c, representing the fraction of Brillouin contribution to the magnetization was not fixed. The value of c could be increased up to ca. 0.5 without significant deterioration of the fit with the Langevin function, as is shown by the solid line in Fig. 4. The presence of 50 percent of paramagnetic species in the iron(III) doped xerogel is in agreement with the Mössbauer spectra at 4.2 K, see below. The equally good fits with equation 5 yields M_s values between 6.4 and 3.1 Am^2/kg and particle radii of between 1.2 and 1.5 nm for c varying between 0 and 0.5. Hence, the field dependence of the magnetization at 5 K may be understood by assuming that the iron(III) doped xerogel consists of a mixture of small superparamagnetic particles with a radius of 1.3 ± 0.2 nm and of isolated paramagnetic iron(III) ions, in an approximately 50:50 ratio. A similar small radius of 1 to 5 nm was reported [7] for iron(III) species deposited in mesoporous silica aerogels. The very small radius of the superparamagnetic particles may indicate that they are formed by clusters of several iron(III) oxide molecules or several $Fe(acac)_3$ molecules which are encapsulated within the Fe-3 xerogel.

A similar magnetic behavior and size was reported [16] for iron-doped siloxane-polyoxyethylene nanocomposites prepared through a sol-gel method. Indeed, particles with an average radius of 6 and 10.5 nm were prepared and

the temperature dependence of their susceptibility and the field dependence of their magnetization were found to be quite similar to those shown in Figs 3 and 4. Specifically, the magnetic susceptibility of the smallest particles shows a typical paramagnetic Curie law behavior, whereas the zero field cooled and field cooled magnetic susceptibility of the largest particles depart at ca. 32 K. The 5 K magnetization of both particles does not saturate in a field of 5 T. This magnetic behavior results from the coexistence of very small clusters of iron(III) ions and of blocked nanoparticles, a mixture that is similar to the mixture observed herein.

The 5 K magnetization curve shown in Fig. 4 differs markedly from the hysteresis loops obtained [10, 11] on iron oxide doped aerogels and xerogels, loops that show substantial coercive fields of ca. 0.2 T. However, none ot the aerogel or xerogel samples exhibit saturation of their magnetization under 6 T. In contrast, the unheated iron oxide aerogel prepared by Cannas, et al. [17] behaves like a weak paramagnet at 295 K, with no coercivity nor saturation, and thus is similar to the sample understudy herein, see Fig. 4.

The diversity of magnetic behavior observed for iron(III) doped aerogels and xerogels results no doubt from the nature of the iron species embedded in the gel pores, its concentration, the size of any nanoparticles, and the existence or absence of interactions between these particles. The absence of a maximum in the temperature dependence of the magnetization and of saturation in the 5 K magnetization curve indicate that the iron(III) doped xerogel studied herein contains superparamagnetic particles of less than ca. 5 nm that are not interacting. Further, the dominant paramagnetic behavior of the xerogel indicates that part of the iron species are paramagnetic down to 4.2 K. This conclusion is supported by Mössbauer spectral measurements, see below.

3.3. Mössbauer spectral studies

The Mössbauer spectra of the Fe-1 iron(III) doped silica xerogel have been measured between 4.2 and 295 K. Between 85 and 295 K the spectra exhibit a broadened quadrupole doublet that has been fit either with an asymmetric quadrupole doublet with lines of the same line width but different area, see the hyperfine parameters given in Table I, or with a distribution [18] of quadrupole doublets that has a linear correlation with the isomer shifts, as is shown in Fig. 5. In the distribution fits the line width has been constrained to 0.28 mm/s. For each quadrupole doublet component in the distribution fit there is a corresponding isomer shift. The average value of the isomer shift indicates that iron(III) is present in the doped silica xerogel. The significant quadrupole splitting is also consistent [19, 20] with the presence of iron(III) ions in a distorted Si–O environment. The distribution of isomer shifts and quadrupole splittings results from the variety of local environments that the iron(III) ions experience in the amorphous xerogel. The average isomer shift and quadrupole shift given in Table I are in complete agreement with those previously observed in iron oxide doped aerogels and xerogels [10–12, 17].

Between 4.2 and 70 K, in addition to the broadened quadrupole doublet, the Mössbauer spectra also exhibit a highly broadened magnetic sextet and a second less broadened magnetic sextet with a larger hyperfine field. The one doublet and two sextet model is purely phenomenological and is the simplest model that gives a reasonable fit of the spectra. The results of the fits with these three components are shown in Fig. 6 and the spectral parameters are given in Table I. The temperature dependence of the spectra shown in Fig. 6 is quite different from those previously reported [10, 11, 17]. Specifically, the sextet with a hyperfine field of ca. 52 T appears with a fully developed field at 70 K and its area increases only moderately between 70 and 4.2 K. No extreme broadening of the sextet lines is observed in Fig. 6 in contrast with the strong broadening previously observed [10, 11, 17]. The Mössbauer spectra indicate that the nanocomposite material prepared herein starting from $Fe(acac)_3$ differs from those previously prepared [10, 11, 17] starting with iron nitrate, either in the nature of the embedded iron species or, more likely, in the interactions between the iron nanoparticles embedded in the gel.

At 4.2 K the doublet has a relative area of ca. 40 percent indicating that ca. 40 percent of the iron(III) is superparamagnetic or paramagnetic, in agreement with the analysis of the magnetization results, see above. The two sextets, with a total relative area of ca. 60 percent, may be assigned to small magnetic particles which are relaxing on the Mössbauer time scale of 10^{-8} to 10^{-9} s. Above 70 K, the Mössbauer blocking temperature, the particles are rapidly relaxing on the Mössbauer time scale and contribute [21] to the observed doublet, see Fig. 5a. Below 70 K the particles are relaxing slowly on the Mössbauer time scale and contribute to the observed sextets, see Fig. 6, whose hyperfine fields are almost temperature independent, as would be expected of superparamagnetic particles of a given size [21, 22].

The ca. 52 T hyperfine field of the less broadened sextet is characteristic of iron(III) oxides [11, 23]. The hyperfine parameters measured at 4.2 K are compatible with virtually any of the iron(III) oxides [11] and could result from a mixture of these oxides. All the iron(III) oxides and hydroxides [10–12, 16, 24], α-Fe_2O_3, γ-Fe_2O_3, $Fe_5HO_8.4H_2O$, amorphous Fe_2O_3, Fe_3O_4, α-FeOOH, and γ-FeOOH. have been identified by various methods in iron(III) doped aerogels or xerogels and it is not possible to uniquely assign the observed broadened sextet to a given iron(III) oxide. As was shown by Casas *et al*. [11], Mössbauer experiments in an applied field may help to separate the contributions from the different iron oxides, hematite or α-Fe_2O_3, maghemite or γ-Fe_2O_3, ferrihydride or $Fe_5HO_8.4H_2O$, or amorphous Fe_2O_3.

The assignment of the sextet with the lower hyperfine field of ca. 20 T is even more difficult. In the analysis of the 5 K Mössbauer spectrum of their sample T, a sample

that is rather similar to our sample Fe-1, Predoi *et al*. [12] assign a broad sextet with a hyperfine field of 28 T and an isomer shift of 0.9 mm/s to a non-stoichiometric fayalite, Fe_2SiO_4. Fits of the spectra in Fig. 6 were successfully carried out with such hyperfine parameters. However, the percent area of ca. 40 percent observed for this sextet at all temperatures between 4.2 and 70 K is very large. Further, in view of the Néel temperature of 66 K of fayalite [25] its presence as a sextet in the 70 K spectrum is problematic. Finally, above 70 K, fayalite should give rise to a quadrupole doublet with a large isomer shift and a large quadrupole splitting characteristic of high-spin iron(II). The absence of such a doublet in Fig. 5 exludes the presence of any fayalite in sample Fe-1.

The sextet with the lower hyperfine field of ca. 20 T may result from particles relaxing with an intermediate relaxation rate, comparable to the Mössbauer time scale or, alternatively may result from iron(III) ions at or near the surface of the nanoparticles [26]. An approximate calculation based on the structure of α-Fe_2O_3, indicates that about 30% of the iron(III) ions reside in a shell of 0.1 nm thickness on the interface with the xerogel of a particle with a radius of 1.3 nm. The physical meaning of this sextet should not be taken too strictly because this sextet is introduced in the fit to reproduce the experimental spectrum but may be an artefact of the simple fitting model. The coexistence of the doublet and the two sextets indicate the presence of particles with different sizes [22, 27].

Because sample Fe-1 was heated only to 423 K, one may wonder whether undecomposed $Fe(acac)_3$ may be present in the xerogel. The Mössbauer spectral hyperfine parameters of these particles do not correspond to those observed [28, 29] for crystalline $Fe(acac)_3$ but the paramagnetic hyperfine parameters would be consistent with non-crystalline $Fe(acac)_3$ dispersed in a xerogel. However, the optical absorption spectrum of the Fe-1 iron(III) doped xerogel is very different from that of crystalline $Fe(acac)_3$. Thus both the Mössbauer spectral studies and the optical absorption spectra indicate that the heating of this xerogel to 423 K has likely decomposed the $Fe(acac)_3$ starting material.

Fits of the temperature dependence of the logarithm of the Mössbauer spectral absorption area and the isomer shift with the Debye model for a solid, see Fig. 7, yield Debye temperatures, θ_D, of 246(11) and 350(25) K, respectively. These values are much lower than those typical of macroscopic crystals, i.e., a θ_D, value of 500 K is observed [26] for α-Fe_2O_3, and the small values indicate a soft lattice with many voids in the iron(III) environment of the doped silica xerogel.

Finally, the 295 K Mössbauer spectrum of sample Fe-2 was obtained. However, because of the thickness of the block and its low iron content, the signal to noise ratio of this spectrum is low. The spectrum consists of a broad quadrupole doublet with and isomer shift of 0.27(1) mm/s and a quadrupole splitting of 0.62(3) mm/s. These values are significantly different from those reported for Fe-1 in Table I but are in the range observed for iron(III) in a silica matrix. Hence, the drying mode of the gel also affects the average iron Si–O environment and hence the hyperfine parameters.

3.4. The blocking temperature

The superparamagnetic relaxation time is given by

$$\tau = \tau_0 e^{KV/kT}, \tag{6}$$

where K is the magnetic anisotropy energy per unit volume of material, V is the volume of the individ-

TABLE I Mössbauer spectral hyperfine parameters for the iron(III) doped silica xerogel

T, (K)	H, (T)	δ, (mm/s)[a]	ΔEQ_b, (mm/s)	Γ, (mm/s)	*Area*, (%ε)(mm/s)	*Area*, (%)
295	0	0.372	0.86	0.71	− 4.102	100
225	0	0.426	0.88	0.72	− 4.553	100
155	0	0.459	0.90	0.72	− 6.409	100
85	0	0.493	0.90	0.72	− 6.469	100
70	51.8	0.492	0.00	1.81	− 3.195	24
	20.4	0.492	0.00	3.45	− 3.166	24
	0	0.492	0.90	0.77	− 7.197	52
60	52.3	0.495	0.00	1.69	− 3.565	25
	20.9	0.495	0.00	3.31	− 3.816	26
	0	0.495	0.92	0.74	− 7.028	49
40	52.0	0.490	0.00	1.59	− 4.364	29
	21.4	0.490	0.00	3.12	− 3.823	25
	0	0.490	0.91	0.75	− 6.947	46
20	52.3	0.490	0.00	1.54	− 4.954	31
	21.9	0.490	0.00	2.82	− 4.182	26
	0	0.490	0.92	0.73	− 7.077	43
4.2	52.1	0.492	0.00	1.52	− 5.721	35
	23.1	0.492	0.00	2.60	− 4.105	25
	0	0.492	0.96	0.71	− 6.556	40

[a]The isomer shifts are given to room temperature α-iron foil.
[b]The quadrupole splitting for the doublets and the quadrupole shifts for the sextets.

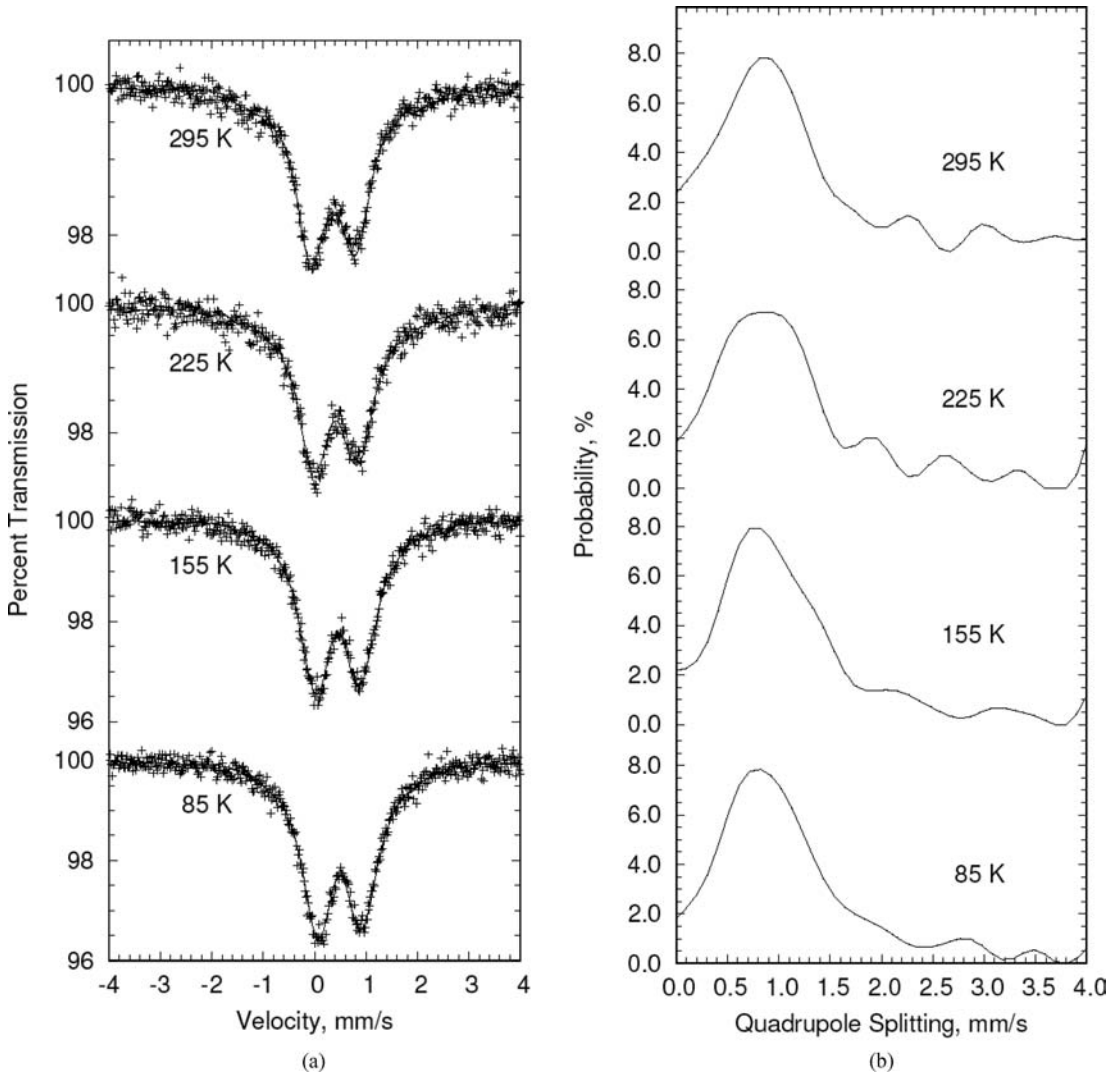

Figure 5 The Mössbauer spectra of the iron(III) doped silica xerogel measured between 85 and 295 K and fit with a distribution of quadrupole doublets, (a), and the corresponding distribution, (b).

ual particles, k is the Boltzmann constant, and T is the temperature. The value of τ_0, is related to the gyromagnetic precession frequency and is in the range [30] of 10^{-9} to 10^{-13} s.

Typically, in Mössbauer spectroscopy, the blocking temperature, T_B, is taken to be the temperature at which the magnetically split and the magnetically unsplit spectral components have equal areas. For the iron(III) doped silica xerogel the observed blocking temperature is ca. 70 K and the average radius, as determined from the mass magnetization, is 1.3(2) nm. At this temperature, the average relaxation time of the particles is equal to the characteristic Mössbauer time scale taken to be 10^{-8} s. By using a τ_0 value of 10^{-9} s, a magnetic anisotropy energy of 2.4×10^5 J/m^3 is obtained from equation 6. Similar large values, values approximately ten times larger than the bulk magnetic anisotropy energies measured for iron oxides, have been reported [31] for 4 nm particles of γ-Fe_2O_3 prepared by the sol-gel method and attributed to interparticle dipolar interactions. A large increase in the magnetic anistropy energy of ferrihydrite from 6×10^3 to 4×10^4 J/m^3 has been reported [32] for nanoparticles whose average size decreases from 6 to 3 nm. Hence, for the very small particles of ca. 1.3 nm observed herein, a large magnetic anisotropy energy is not unexpected.

The observed blocking temperature depends upon the different time scales of the different experimental techniques used. Magnetic measurements have a characteristic time of 10 s, a time that is much larger than the Mössbauer characteristic time [30–33] of 10^{-8} s. By using this time and the magnetic anisotropy energy determined above, a value of 6 ± 2 K is obtained as an estimate of the blocking temperature that would be observed by magnetic measurements in a field cooled/zero field cooled experiment. Hence, it is not surprising that no parting of the field cooled/zero field cooled magnetization was observed down to 4.2 K in Fig. 3, where, further, the magnetic behavior is dominated by the paramagnetic contribution. Such a low blocking temperature as predicted for magnetic measurements on the 1.3 nm iron(III)-doped xerogel

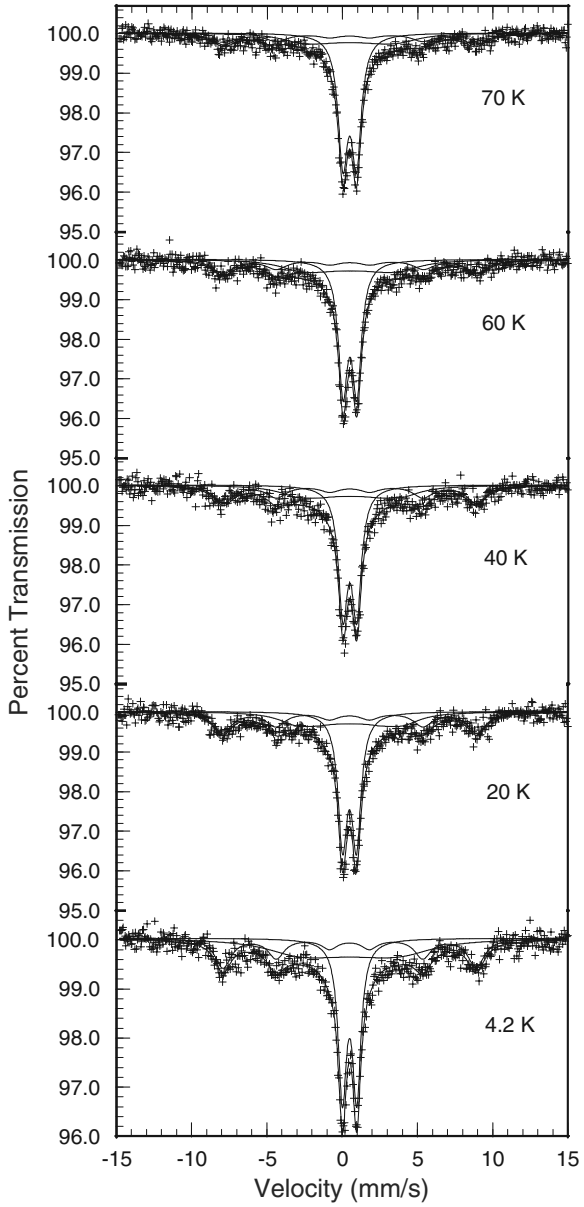

Figure 6 The Mössbauer spectra of the iron(III) doped silica xerogel measured between 4.2 and 70 K and fit with a broadened quadrupole doublet and two magnetic sextets.

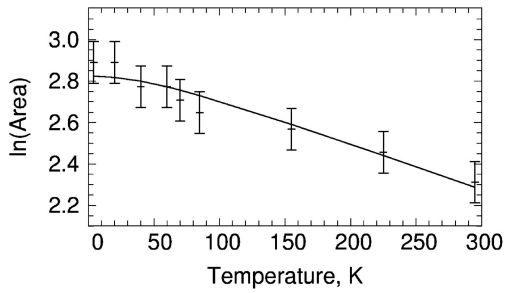

Figure 7 The temperature dependence of the logarithm of the Mössbauer spectral absorption area, top, and the isomer shift, bottom, fit with the Debye model for a solid.

particules is in agreement with the blocking temperatures of 32 K measured [16] for 6 nm iron-doped siloxane-polyoxyethylene nanocomposites prepared by the sol-gel process.

4. Conclusions

An iron(III) doped xerogel has been synthesized by the sol-gel technique, by using $Fe(acac)_3$ as the iron(III) precursor. The *Z*-scan method has been used to determine the nonlinear refractive index, n_2 of -1.95×10^{-11} cm^2/W for a transparent monolithic xerogel. A significant nonlinear refraction was observed with a weak contribution arising from nonlinear absorption and a strong contribution arising from a reorganization of the delocalized electrons of the acetylacetonate ligands or the charge of the oxide dianions toward the iron(III) ions in the presence of a strong polarized laser beam, a reorganization that occurs because of the soft xerogel lattice revealed by the Mössbauer spectral measurements. The temperature dependence of the magnetic susceptibility, the 5 K field dependence of the magnetization, and the 4.2 K Mössbauer spectra are compatible with the coexistence of small clusters or superparamagnetic iron(III) oxide particles with an average radius of 1.3 ± 0.2 nm and of isolated paramagnetic iron(III) ions in an approximate ratio of 50:50. A large magnetic anisotropy energy of 2.4×10^5 J/m^3 is obtained from the blocking temperature of 70 K measured in Mössbauer spectroscopy.

Acknowledgments

The authors would like to thank both the Centre d'Optique Photonique et Lasers, Université Laval, Québec, for help with the nonlinear optical measurements and for the use of its femtosecond mode-locked fiber laser and Drs. J. R. Long and L. Berben of the Department of Chemistry, University of California—Berkeley, for help with the SQUID measurements. This work is part of a cooperative program between Wallonie-Bruxelles and Québec, a program that was supported by the Ministère de la Région Wallonne-Direction des Relations Internationales, Belgium. The authors acknowledge with thanks the financial support of the Fonds National de la Recherche Scientifique, Belgium, through grants 9.456595 and the Ministère de la Région Wallonne for grant RW/115012. This work was also supported by the Action de Recherche Concertée 00/05-265 of the Communauté Française de Belgique and the Ministère de la Région Wallonne, DGTRE, Belgium. M.-J. Hubin-Franskin acknowledges support from the Fonds National de la Recherche Scientifique, Belgium, as a Directeur de Recherches.

References

1. R. L. SUTHERLAND, in "Handbook of Nonlinear Optics" (Marcel Dekker, New York, 1996).

2. B. E. A. SALEH and M. C. TEICH, "Fundamentals of Photonics" (Wiley, New York, 1991).
3. P. N. PRASAD and D. J. WILLIAMS, "Introduction to Nonlinear Optical Effects in Molecules and Polymers" (Wiley, New York, 1991).
4. E. I. KO, in "Handbook of Heterogeneous Catalysis," edited by G. Ertl, H. Knözinger and J. Weitkamp (Wiley-VCH, Weinheim, 1997) Vol. 1, p. 86.
5. R. D. GONZALEZ, T. LOPEZ and R. GOMEZ, *Catal. Today* **35** (1997) 293.
6. S. LAMBERT, C. CELLIER, P. GRANGE, J. P. PIRARD and B. HEINRICHS, *J. Catal.* **221** (2004) 335.
7. C. T. WANG and A. H. RO, *Appl. Catal. A* **285** (2005) 196.
8. I. COROIU, E. CULEA and AL. DARABONT, *J. Magn. Magn. Mater.* **290–291** (2005) 997.
9. C. J. BRINKER and G. W. SCHERER, "In Sol-Gel Science: The Physics and Chemistry of Sol-Gel Processing" (Academic Press, San Diego, 1990).
10. C. CANNAS, M. F. CASULA, G. CONCAS, A. CORRIAS, D. GATTESCHI, A. FALQUI, A. MUSINU, C. SANGREGORIO and G. SPANO, *J. Mater. Chem.* **11** (2001) 3180.
11. LL. CASAS, A. ROIG, E. MOLINS, J. M. GRENÈCHE, J. ASENJO and J. TEJADA, *Appl. Phys. A* **74** (2002) 591.
12. D. PREDOI, V. KUNCSER, M. ZAHARESCU, W. KEUNE, B. SAHOO, M. VALEANU, M. CRISAN, M. RAILEANU, A. JITIANU and G. FILOTI, *Phys. Stat. Sol. (c)* **1** (2004) 3507.
13. M. SHEIK-BAHAE, A. A. SAID, T. H. WEI, D. J. HAGAN and E. W. VAN STRYLAND, *IEEE J. Quantum Electronics* **26** (1990) 760.
14. V. ROSSO, J. LOICQ, Y. RENOTTE and Y. LION, *J. Non-Cryst. Solids*, **342** (2004) 140.
15. M. CASON, D. BERSANI, G. ANTONIOLI, P. P. LOTTICI, A. MONTENERO and M. CAVALLI, *Opt. Mater.* **12** (1999) 447.
16. L. A. CHIAVACCI, K. DAHMOUCHE, N. J. O. SILVA, L. D. CARLOS, V. S. AMARAL, V. DE ZEA BERMUDEZ, S. H. PULCINELLI, C. V. SANTILLI, V. BRIOIS and A. F. CRAIEVICH, *J. Non-Cryst. Solids* **345–346** (2004) 585.
17. C. CANNAS, G. CONCAS, F. CONGIU, A. MUSINU, G. PICCALUGA and G. SPANO, *Z. Naturforsch.* **57a** (2002) 154.
18. G. LE CAËR and J. M. DUBOIS, *J. Phys. E* **12** (1979) 1083.
19. S. RAMESH, I. FELNER, Y. KOLTYPIN and A. GEDANKEN, *J. Mater. Res.* **15** (2000) 944.
20. N. MAXIM, A. OVERWEG, P. J. KOOYMAN, J. H. M. C. VAN WOLPUT, R. W. J. M. HANSSEN, R. A. VAN SANTEN and H. C. L. ABBENHUIS, *J. Phys. Chem. B* **106** (2002) 2203.
21. S. MØRUP, In "Paramagnetic and Superparamagnetic Relaxation Phenomena Studied by Mössbauer Spectroscopy" (Polyteknisk Forlag, 1981).
22. M. L. WADE, D. G. AGRESTI, T. J. WDOWIAK, L. P. ARMENDAREZ and J. D. FARMER, *J. Geophys.* **104** (1999) 8489.
23. E. MURAD and J. H. JOHNSTON, in "Mössbauer Spectroscopy Applied to Inorganic Chemistry," edited by G. J. Long (Plenum Press, New York, 1987) Vol. 2, p. 507; E. MURAD, L. H. BOWEN, G. J. LONG and T. G. QUIN, *Clay Minerals.* **23** (1988) 161.
24. J. W. LONG, M. S. LOGAN, C. P. RHODES, E. E. CARPENTER, R. M. STROUD and D. R. ROLISON, *J. Am. Chem. Soc.* **126** (2004) 16879.
25. W. LOTTERMOSER, K. FORCHER, G. AMTHAUER and H. FUESS, *Phys. Chem. Min.* **22** (1995) 259.
26. F. BÖDKER, S. MØRUP, C. A. OXBARROW, S. LINDEROTH, M. B. MADSEN and J. W. NIEMANTSVERDRIET, *J. Phys.: Condens. Matter* **4** (1992) 6555.
27. P. V. HENDRIKSEN, F. BÖDKER, S. LINDEROTH, S. WELLS and S. MØRUP, *J. Phys.: Condens. Matter.* **6** (1994) 3081.
28. J. W. G. WIGNALL, *J. Chem. Phys.* **44** (1966) 2462.
29. G. M. BANCROFT, A. G. MADDOCK, W. K. ONG, R. H. PRINCE and A. J. STONE, *J. Chem. Soc. (A)* (1967) 1966.
30. E. TRONC, *Il Nuovo Cimento* **18D** (1996) 163.
31. D. PREDOI, V. KUNCSER, E. TRONC, M. NOGUES, U. RUSSO, G. PRINCIPI and G. FILOTI, *J. Phys.: Cond. Matter* **15** (2003) 1797.
32. S. M. DUBIEL, B. ZABLOTNA-RYPIEN, J. B. MACKEY and J. M. WILLIAMS, *Biophys. J.* **28** (1999) 263.
33. G. XIAO, S. H. LIOU, A. LEVY, J. N. TAYLOR and C. L. CHIEN, *Phys. Rev. B* **34** (1986) 7573.

Received 16 November 2004
and accepted 31 October 2005